Dominik Lips, Artem Ryabov and Philipp Maass*

Nonequilibrium Transport and Phase Transitions in Driven Diffusion of Interacting Particles

https://doi.org/10.1515/zna-2020-0028
Received January 24, 2020; accepted February 14, 2020

Abstract: Driven diffusive systems constitute paradigmatic models of nonequilibrium physics. Among them, a driven lattice gas known as the asymmetric simple exclusion process (ASEP) is the most prominent example for which many intriguing exact results have been obtained. After summarising key findings, including the mapping of the ASEP to quantum spin chains, we discuss the recently introduced Brownian ASEP (BASEP) as a related class of driven diffusive system with continuous space dynamics. In the BASEP, driven Brownian motion of hardcore-interacting particles through one-dimensional periodic potentials is considered. We study whether current–density relations of the BASEP can be considered as generic for arbitrary periodic potentials and whether repulsive particle interactions other than hardcore lead to similar results. Our findings suggest that shapes of current–density relations are generic for single-well periodic potentials and can always be attributed to the interplay of a barrier reduction, blocking, and exchange symmetry effect. This implies that in general up to five different phases of nonequilibrium steady states are possible for such potentials. The phases can occur in systems coupled to particle reservoirs, where the bulk density is the order parameter. For multiple-well periodic potentials, more complex current–density relations are possible, and more phases can appear. Taking a repulsive Yukawa potential as an example, we show that the effects of barrier reduction and blocking on the current are also present. The exchange symmetry effect requires hardcore interactions, and we demonstrate that it can still be identified when hardcore interactions are combined with weak Yukawa interactions. The robustness of the collective dynamics in the BASEP with respect to variations of model details can be a key feature for a successful observation of the predicted current–density relations in actual physical systems.

Keywords: Brownian Asymmetric Simple Exclusion Process; Driven Diffusion; Nonequilibrium Dynamics; Nonequilibrium Phase Transitions; Single-File Transport.

1 Introduction

Driven diffusive systems of interacting particles constitute an important class of systems to study fundamental aspects of nonequilibrium physics. This holds in particular for one-dimensional models, where exact analytical derivations are possible or reliable approximations are known, for example, when information about exact equilibrium properties can be utilised for the treatment of nonequilibrium states.

A prominent model in the field of driven diffusive systems is the asymmetric simple exclusion process (ASEP), where particles hop between nearest-neighbour sites of a lattice with a bias in one direction and where the sole interaction between particles is a mutual site exclusion, implying that a lattice site cannot be occupied by more than one particle [1, 2]. In the ASEP on a one-dimensional lattice with L sites and periodic boundary conditions, i.e. a ring of L sites, particles jump to vacant nearest-neighbour sites with rates Γ_+ and Γ_- in clockwise and counterclockwise direction, respectively, where $\Gamma_+ > \Gamma_-$ for a bias in clockwise direction. In a corresponding open system with L sites, where the leftmost and rightmost lattice site can exchange particles with reservoirs L and R, respectively, additional rates $\Gamma_{\rm in}^{\rm L}$, $\Gamma_{\rm in}^{\rm R}$ and $\Gamma_{\rm out}^{\rm L}$, $\Gamma_{\rm out}^{\rm R}$ specify the corresponding rates for particle injection and ejection. Many properties of the ASEP can be inferred from the even simpler totally asymmetric simple exclusion process (TASEP) with unidirectional transport ($\Gamma_- = 0$).

Stochastic processes in driven lattice gases are described by a master equation for the probabilities of particle configurations, which can be viewed also as the occupation number representation of a Schrödinger equation in imaginary time [3, 4]. This leads to some interesting connections to quantum systems with in

***Corresponding author: Philipp Maass,** Universität Osnabrück, Fachbereich Physik, Barbarastraße 7, D-49076 Osnabrück, Germany, E-mail: maass@uos.de. https://orcid.org/0000-0002-1268-8688
Dominik Lips: Universität Osnabrück, Fachbereich Physik, Barbarastraße 7, D-49076 Osnabrück, Germany, E-mail: dlips@uos.de. https://orcid.org/0000-0003-2912-5416
Artem Ryabov: Charles University, Faculty of Mathematics and Physics, Department of Macromolecular Physics, V Holešovičkách 2, CZ-18000 Praha 8, Czech Republic, E-mail: rjabov.a@gmail.com. https://orcid.org/0000-0001-8593-9516

Published online April 8, 2020

general non-Hermitian Hamilton operator H [2, 3, 5, 6]. As an example, we recapitulate in the Appendix the connection of the ASEP with periodic boundary conditions to the *XXZ* quantum spin chain with non-Hermitian boundary conditions [6]. Spin chains are often used to study fundamental aspects of nonequilibrium quantum physics. Several examples related to current problems, in particular to questions of equilibration in nonintegrable spin chain models, can be found in this special issue on the physics of non-equilibrium systems.

The ASEP has been intensively studied in the past. Let us summarise here some of the most important findings for the ASEP and variants of it:

- Using the Bethe ansatz for corresponding quantum spin chain models, or a construction in terms of matrix product states, exact results for microstate distributions in nonequilibrium steady states (NESSs) could be derived [1, 2, 7]. Matrix product states in principle exist for driven lattice gases with arbitrary nearest-neighbour interactions [8], although their explicit construction may be difficult.
- Based on the exact approaches for deriving distribution of microstates in NESS, large deviation functions for fluctuations of time-averaged densities and currents were derived [9–11]. They have been computed also for coarse-grained descriptions by the macroscopic fluctuation theory [12]. Large deviation functions are argued to play a similar role for time-averaged quantities in NESS as the free energy in equilibrium systems [13]. They can exhibit singularities [14–17], sometimes referred to as "dynamical phase transitions," which for certain classes of systems are caused by a violation of an "additivity principle" [18].
- The Bethe ansatz turned out to be a valuable tool also for deriving microstate distributions of nonsteady states [19, 20]. The propagator for the microstate time evolution in the ASEP was related to integrated Fredholm determinants [21] and led to the derivation of the Tracy–Widom distribution of random matrix theory for the asymptotic behaviour in case of a step initial condition [22]. This result generalised an earlier one derived for the TASEP [23] and proved that the propagation of density fluctuations in the ASEP belongs to the Kardar–Parisi–Zhang (KPZ) universality class [24].
- In open systems coupled to particle reservoirs, phase transitions between NESS occur [25–28], where, upon change of control parameters characterising the system-reservoir couplings, the bulk density ρ_b changes discontinuously, or its derivative with respect to the control parameters. Knowing the density dependence of the steady-state bulk current $j_\mathrm{ss}(\rho)$, e.g. from results for a system with periodic boundary conditions, all possible NESS phases with bulk density ρ_b are predicted by the extremal current principles [25, 27, 29]:

$$\rho_\mathrm{b} = \begin{cases} \underset{\rho_- \le \rho \le \rho_+}{\operatorname{argmin}} \{j_\mathrm{ss}(\rho)\}\,, & \rho_- \le \rho_+\,, \\ \underset{\rho_+ \le \rho \le \rho_-}{\operatorname{argmax}} \{j_\mathrm{ss}(\rho)\}\,, & \rho_+ \le \rho_-\,. \end{cases} \tag{1}$$

Here ρ_- and ρ_+ can be any densities bounding a monotonically varying region encompassing the plateau part with bulk density ρ_b (which may strictly exist only in the thermodynamic limit of infinite system size). Which of the phases predicted by (1) really occurs for a given control scheme of system-reservoir couplings is given by the dependence of ρ_- and ρ_+ on respective control parameters.

The extremal current principles can be reasoned based on the consideration of shock front motions [27, 29, 30] or by resorting to a decomposition of the steady-state current into its drift and diffusive part inside the region of monotonically varying density profile [25]. Because these reasonings do not require specific properties of the ASEP, they are quite generally valid for driven diffusive systems coupled to particle reservoirs. This includes driven lattice gases with interactions other than site exclusion [30–33], systems with continuous space dynamics, and systems with periodic space structure and/or time-periodic driving, when considering period-averaged densities [34]. For specific system-reservoir couplings termed "bulk-adapted," it is possible to parameterise the exchange of particles by reservoir densities such that all possible NESS phases must appear. The bulk-adapted couplings can be determined by a general method for driven lattice gases with short-range interactions [33, 34].

- For random and non-Poissonian hopping rates, Bose–Einstein–type condensations of vacancies can occur in front of the slowest particle with the smallest jump rate [35, 36].
- Coarse-grained continuum descriptions of the ASEP and of multilane variants [37] give rise to an infinite discrete family of nonequilibrium universality classes in nonlinear hydrodynamics, where density fluctuations spread in time by power laws with exponents given by the Kepler ratios of consecutive Fibonacci numbers [38]. This includes the KPZ class, for which an exact expression for the scaling function was derived [39]. Predictions of the theory of fluctuating nonlinear hydrodynamics were recently confirmed in an exact treatment by considering a two-species exclusion process [40].

As for applications, the ASEP appears as a basic building block in manifold descriptions of biological traffic [41, 42]. In fact, the ASEP was introduced first to describe protein synthesis by ribosomes [43], and it is frequently used in connection with the motion of motor proteins along microtubules or actin tracks [44, 45]. An in vitro study with fluorescently labelled single-headed kinesin motors moving along a microtubule provided experimental evidence for a state of coexisting phases with different motor densities [46]. Other applications concern vehicular traffic [47, 48], diffusion of ions through cell membranes [49] and of molecules through nanopores [50, 51], and electron transport along molecular wires in the incoherent classical limit [52, 53]. However, a direct experimental realisation of the ASEP is difficult, because of its discrete nature. Hence, it is important to see whether the nonequilibrium physics in the ASEP is reflected in models with continuous space dynamics.

For a single particle, it is well known that effective hopping transport emerges from an overdamped Brownian motion in a periodic potential with amplitude much larger than the thermal energy. The particle can be viewed to jump between neighbouring wells on a coarse-grained time scale with a rate determined by the inverse Kramers time [54]. One is thus led to ask whether the driven diffusion of many hardcore-interacting particles in a periodic energy landscape can reflect the driven lattice gas dynamics in the ASEP. To answer this question, we recently introduced a corresponding class of nonequilibrium processes termed Brownian ASEP (BASEP) [55, 56], where hard spheres with diameter σ are driven through a periodic potential with wavelength λ by a constant drag force f. For a sinusoidal external potential, we found that the current–density relation of the ASEP is indeed recaptured in the BASEP, but only for a limited range of particle diameters σ. For other σ, quite different behaviours are obtained.

The nonequilibrium physics of the BASEP should be explorable directly by experiment, for example, in setups utilising advanced techniques of microfluidics and optical and/or magnetic micromanipulation [57–61]. This includes arrangements where the particles are driven by travelling-wave (TW) potentials [62]. Many of the new collective transport properties seen in the BASEP can be even identified by studying local dynamics of individual transitions between potential wells [63].

In this work, we address the question how the current–density relations found for the BASEP in a sinusoidal external potential are affected when considering different external potentials and short-range interactions other than hardcore exclusions. Our investigation for the different external potentials is carried out based on the small-driving approximation introduced in [55] and [56]. With respect to short-range interactions other than hardcore exclusions, we focus on a Yukawa pair potential. It is shown that the current–density relation for single-well periodic potentials and for the Yukawa interaction has similar features as that of the BASEP. This suggests that the BASEP can serve as a reference model for a wide class of external periodic potentials and pair interactions.

In addition, we extend a former analysis to prove that current reversals cannot occur in systems driven by a constant drag and by travelling waves. These proofs are based on an exact calculation of the total entropy production in corresponding NESS for particles with arbitrary pair interactions. Current reversals refer to steady states, where particle flow is opposite to the external bias. They were reported for lattice models [34, 64–67] and were recently found experimentally in a rocking Brownian motor [59]. Their absence in TW driven systems was conjectured based on simulation results and a perturbative expansion of the single-particle density in the NESS around its period-averaged value [68].

The article is organised as follows. In Section 2, Current–Density Relations: Analytical Results, we present an analytical treatment of densities and currents for the overdamped one-dimensional Brownian motion of particles with arbitrary pair interactions. This section partly summarises results presented earlier [55, 56] and introduces the small-driving approximation used subsequently for our investigation of hardcore-interacting particles. It also contains our proofs on the absence of current reversals for general pair interactions. In Section 3, Hardcore Interacting Particles in Harmonic Potential, we outline our findings for the BASEP with sinusoidal external potential, and in Section 4, Impact of External Periodic Potential, we contrast them with results for a Kronig–Penney and triple-well periodic potential. In Section 5, Impact of Interactions Other Than Hardcore Exclusions, we discuss our results for the Yukawa interaction. Section 6, Summary and Conclusions, concludes the article with a summary and outlook.

2 Current–Density Relations: Analytical Results

The overdamped single-file Brownian motion of N particles in a periodic potential $U(x) = U(x+\lambda)$ with pair interaction under a constant drag force f is described by the

Langevin equations:

$$\frac{\mathrm{d}x_i}{\mathrm{d}t} = \mu\left(f + f_i^{\mathrm{int}} - \frac{\partial U(x_i)}{\partial x_i}\right) + \sqrt{2D}\,\eta_i(t), \qquad (2)$$

where μ and $D = \mu k_{\mathrm{B}}T$ are the bare mobility and diffusion coefficient, $k_{\mathrm{B}}T$ is the thermal energy, and f_i^{int} is the interaction force on the i^{th} particle. The $\eta_i(t)$ are independent and δ-correlated Gaussian white noise processes with zero mean and unit variance, $\langle\eta_i\rangle = 0$ and $\langle\eta_i(t)\eta_j(t')\rangle = \delta_{ij}\delta(t - t')$. Unless noted otherwise, we consider closed systems with periodic boundary conditions, which means that the particles are dragged along a ring.

Hardcore interactions imply the boundary conditions $|x_i - x_j| \geq \sigma$, i.e. overlaps between neighbouring particles are forbidden. For the BASEP with only hardcore interactions, these boundary conditions must be taken into account, while the interaction force f_i^{int} can be set to zero in (2). We define the density as a (dimensionless) filling factor of the potential wells, i.e. by $\rho = N/M$, where M denotes the total number of periods of $U(x)$. The system length is $L = M\lambda$, and the number density is ρ/λ. For hardcore-interacting particles of size σ, the filling factor ρ has the upper bound λ/σ.

The joint probability function (PDF) of the particle centre coordinates $\boldsymbol{x} = (x_1, \ldots, x_N)$ evolves in time according to the N-particle Smoluchowski equation[1],

$$\frac{\partial p_N(\boldsymbol{x},\ t)}{\partial t} = -\boldsymbol{\nabla}\cdot\boldsymbol{J}(\boldsymbol{x},\ t), \qquad (3)$$

where the divergence operator acts on the probability current vector $\boldsymbol{J}(\boldsymbol{x},\ t)$ with the i^{th} component given by

$$J_i(\boldsymbol{x}, t) = \mu\left[f - \frac{\partial U(x_i)}{\partial x_i} + f_i^{\mathrm{int}}(\boldsymbol{x})\right] p_N(\boldsymbol{x},\ t) - D\frac{\partial p_N(\boldsymbol{x},\ t)}{\partial x_i}. \qquad (4)$$

The first term describes the drift probability current caused by all forces acting on the i^{th} particle, and the second term gives the diffusive current. The interaction force is assumed to be conservative and due to pair interactions $u^{\mathrm{int}}(x_i,\ x_j)$, i.e. $f_i^{\mathrm{int}}(\boldsymbol{x}) = -\partial U^{\mathrm{int}}(\boldsymbol{x})/\partial x_i$ with

$$U^{\mathrm{int}}(\boldsymbol{x}) = \frac{1}{2}\sum_{i\neq j}^{N} u^{\mathrm{int}}(x_i,\ x_j). \qquad (5)$$

Additional hardcore interactions are not included in the potential (5) but are incorporated into the dynamics by requiring no-flux (reflecting) boundary conditions

$$[J_i(\boldsymbol{x},\ t) - J_{i+1}(\boldsymbol{x},\ t)]|_{x_{i+1}=x_i+\sigma} = 0, \qquad (6)$$

if neighbouring particles hit each other. These boundary conditions ensure conservation of an initial ordering $x_1 < x_2 < \ldots < x_N$ of the particle positions for all times.

2.1 Exact Current–Density Relation

The local density is

$$\varrho(x,\ t) = \left\langle \sum_{i=1}^{N} \delta[x - x_i(t)] \right\rangle, \qquad (7)$$

where the average is taken with respect to the solution of the Smoluchowski equation (3) subject to some initial condition. It satisfies the continuity equation

$$\frac{\partial\varrho(x,\ t)}{\partial t} = -\frac{\partial j(x,\ t)}{\partial x}, \qquad (8)$$

with the particle current density given by [55]

$$j(x,\ t) = \mu[f^{\mathrm{ext}}(x) + f^{\mathrm{int}}(x,\ t)]\,\varrho(x,\ t) - D\frac{\partial\varrho(x\ ,t)}{\partial x}. \qquad (9)$$

Here we introduced the total external force

$$f^{\mathrm{ext}}(x) = f - \frac{\partial U(x)}{\partial x}. \qquad (10)$$

The local interaction force $f^{\mathrm{int}}(x,\ t)$ in (9) is given by

$$f^{\mathrm{int}}(x,\ t) = \frac{1}{\rho(x,\ t)}\int_0^L \mathrm{d}y\, f_2(x,\ y)\rho_2(x,\ y,\ t), \qquad (11)$$

where

$$\varrho_2(x,\ y,\ t) = \left\langle \sum_{i\neq j}^{N} \delta[x - x_i(t)]\ \ \delta[y - x_j(t)] \right\rangle \qquad (12)$$

is the two-point local density, and $f_2(x,\ y)$ is the interaction force of a particle at position y on a particle at position x. It can by expressed as a sum of two distinct contributions:

$$f_2(x,\ y) = k_{\mathrm{B}}T[\delta(y - x + \sigma) - \delta(x - y - \sigma)] - \frac{\partial u^{\mathrm{int}}(x,\ y)}{\partial x}. \qquad (13)$$

The first term is due to a positive and a negative force, if a particle is in contact with other particles at positions

[1] To implement the periodic boundary conditions, we assume an ordered initial configuration $0 \leq x_1 \leq x_2 \ldots \leq x_N < L$ and introduce two fictive particles with enslaved coordinates $x_0 = x_N - L$ and $x_{N+1} = x_1 + L$, which implies $x_N - x_1 < L - \sigma$.

$x-\sigma$ and $x+\sigma$, respectively. We note that the δ functions should not be interpreted as a derivative of a rectangular potential barrier of height $k_\mathrm{B}T$. Instead, they are a consequence of the noncrossing boundary conditions (6) [55]. The amplitude in front of the δ functions must be an energy on dimensional reasons, for which $k_\mathrm{B}T$ is the only relevant scale. It corresponds to the typical collision energy due to the thermal noise. The second term in (13) is the force due to the interaction potential (5).

In the steady state of a closed system with periodic boundary conditions, the density profile is time-independent and periodic, $\varrho_\mathrm{ss}(x+\lambda)=\varrho_\mathrm{ss}(x)$, and the current constant everywhere in the system. It follows directly from (9) [55]

$$j_\mathrm{ss}(\rho,\ \sigma)=\frac{\mu\left[f+\frac{1}{\lambda}\int_0^\lambda \mathrm{d}x\, f_\mathrm{ss}^\mathrm{int}(x)\right]}{\frac{1}{\lambda}\int_0^\lambda \mathrm{d}x\, \varrho_\mathrm{ss}^{-1}(x)}. \tag{14}$$

Up to this point, no approximation has been made. The exact value of the steady-state current (14) depends on both $\varrho_\mathrm{ss}(x)$ and the steady-state limit of the two-point density (12). However, a derivation of the two densities in NESS represents a challenging problem, which can be solved in a few special cases only. Therefore, to proceed further, we need to develop an appropriate approximate theory.

2.2 Small-Driving Approximation

For hardcore interactions, the small-driving approximation (SDA) turned out to be particularly successful in capturing qualitative behaviours of $j_\mathrm{ss}(\rho,\ \sigma)$ [56]. The approximation is carried out in two steps. First, we linearise the current (14) with respect to f,

$$j_\mathrm{ss}(\rho,\ \sigma)\sim\frac{(1+\chi)\mu f}{\frac{1}{\lambda}\int_0^\lambda \mathrm{d}x\, \varrho_\mathrm{eq}^{-1}(x)},\quad f\to 0, \tag{15}$$

where the response coefficient reads

$$\chi=\frac{\partial}{\partial f}\left[\frac{1}{\lambda}\int_0^\lambda \mathrm{d}x\, f_\mathrm{ss}^\mathrm{int}(x)\right]\Bigg|_{f=0}, \tag{16}$$

and, second, we approximate the linear-response expression (15) by setting $\chi=0$.

The ad hoc $\chi=0$ approximation works well in an extended region of particle sizes except for a narrow range $\sigma\approx\lambda/2$ [56]. The equilibrium density profile is obtained by minimising the exact density functional for hard rods [69],

$$\Omega[\varrho(x)]=\int_0^\lambda \mathrm{d}x\ \varrho(x)\Big\{U(x)-\mu_\mathrm{ch} -k_\mathrm{B}T\left[1-\ln\left(\frac{\varrho(x)}{1-\eta(x)}\right)\right]\Big\}, \tag{17}$$

where μ_ch is the chemical potential, and

$$\eta(x)=\int_{x-\sigma}^{x}\mathrm{d}y\ \varrho(y)\,. \tag{18}$$

The minimisation yields the structure equation

$$\begin{aligned}0&=\frac{\delta\Omega[\varrho]}{\delta\varrho}\Bigg|_{\varrho=\varrho_\mathrm{eq}}\\ &=k_\mathrm{B}T\ \ln\left[\frac{\varrho_\mathrm{eq}(x)}{1-\eta_\mathrm{eq}(x)}\right]\\ &\quad+k_\mathrm{B}T\int_x^{x+\sigma}\mathrm{d}y\frac{\varrho_\mathrm{eq}(y)}{1-\eta_\mathrm{eq}(y)}+[U(x)-\mu_\mathrm{ch}],\end{aligned} \tag{19}$$

which we discretised and solved numerically under periodic boundary conditions ($\varrho_\mathrm{eq}(x)=\varrho_\mathrm{eq}(x+\lambda)$). The chemical potential μ_ch was adjusted to give the desired global density (filling factor) $\rho=\int_0^\lambda \mathrm{d}x\ \varrho_\mathrm{eq}(x)$.

2.3 Entropy Production and Absence of Current Reversals

Theory for hardcore-interacting particles with $U^\mathrm{int}(\boldsymbol{x})=0$ was the subject of our previous works on the BASEP [55, 56, 63]. Here we extend the analysis to nonzero $U^\mathrm{int}(\boldsymbol{x})$. We start with considerations related to the total entropy production:

$$\dot{S}_\mathrm{tot}(t)=\dot{S}_\mathrm{sys}(t)+\dot{S}_\mathrm{med}(t)\,, \tag{20}$$

where $\dot{S}_\mathrm{sys}(t)$ and $\dot{S}_\mathrm{med}(t)$ are the entropy production in the system and surrounding medium.

For calculating the time derivative of $S_\mathrm{sys}(t)=-k_\mathrm{B}\int d^N x\ p_N(\boldsymbol{x},\ t)\ln p_N(\boldsymbol{x},\ t)$, we can replace the time derivative of the PDF by the divergence of the current according to (3). After integrating by parts each individual term of the divergence, we get

$$\frac{\dot{S}_\mathrm{sys}(t)}{k_\mathrm{B}}=-\int_\Omega \mathrm{d}^N x\ \boldsymbol{J}(\boldsymbol{x},\ t)\cdot\boldsymbol{\nabla}\ln p_N(\boldsymbol{x},\ t), \tag{21}$$

where Ω is the space of all system microstates consistent with the hardcore constraints. As the next step, we replace $\partial \ln p_N/\partial x_i$ via (4), which gives us two terms

$$\frac{\dot{S}_{\rm sys}(t)}{k_{\rm B}} = \int_\Omega {\rm d}^N x\, \frac{|\boldsymbol{J}(\boldsymbol{x},\ t)|^2}{D p_N(\boldsymbol{x},\ t)} - \int_\Omega {\rm d}^N x\, \frac{\boldsymbol{J}(\boldsymbol{x},\ t)\cdot \boldsymbol{F}(\boldsymbol{x})}{k_{\rm B}T}\,. \tag{22}$$

Here we have introduced the total force $\boldsymbol{F}(\boldsymbol{x})$ with components $F_i(\boldsymbol{x}) = f^{\rm ext}(x_i) + f_i^{\rm int}(\boldsymbol{x})$. The first term is always positive and equal to the total entropy production [70]. The second term, proportional to the mean dissipated power, is the entropy production in the medium.

In the steady state, the system entropy is constant, $\dot{S}_{\rm sys}(t) = 0$, and the total entropy production equal to the entropy produced in the surrounding medium:

$$0 \le \dot{S}_{\rm tot} = \frac{1}{T}\int_\Omega {\rm d}^N x\, \boldsymbol{J}(\boldsymbol{x})\cdot \boldsymbol{F}(\boldsymbol{x}) = \frac{1}{T}\sum_{i=1}^N \int_\Omega {\rm d}^N x\, J_i(\boldsymbol{x})\left[f - \frac{\partial U(x_i)}{\partial x_i} - \frac{\partial U^{\rm int}(\boldsymbol{x})}{\partial x_i}\right]. \tag{23}$$

Here, each single-particle term simplifies after introducing the current density $j_i(x) = \int_\Omega {\rm d}^N x\, J_i(\boldsymbol{x})\delta(x_i - x)$ of the $i^{\rm th}$ particle, and by using that $j_i(x) = j_{\rm ss}/N$ in the steady state, we obtain

$$\int_\Omega {\rm d}^N x\, J_i(\boldsymbol{x})\left[f - \frac{\partial U(x_i)}{\partial x_i}\right] = \frac{j_{\rm ss}}{N} L f. \tag{24}$$

The sum over all interaction forces in (23) yields, after integration by parts,

$$-\sum_{i=1}^N \int_\Omega {\rm d}^N x\, J_i(\boldsymbol{x})\frac{\partial U^{\rm int}(\boldsymbol{x})}{\partial x_i} = \int_\Omega {\rm d}^N x\, U^{\rm int}(\boldsymbol{x})\, \boldsymbol{\nabla}\cdot \boldsymbol{J}(\boldsymbol{x}). \tag{25}$$

Because the divergence of the current is zero in the steady state, this term vanishes. From (23) and (24), we thus obtain the total entropy production in the Onsager form (current times thermodynamic force)

$$\dot{S}_{\rm tot} = \frac{j_{\rm ss} f}{T} L \ge 0. \tag{26}$$

It is extensive in the system size, and the numerator equals the mean heat dissipated at any point of the system in the steady state. As a consequence of the inequality in (26), the steady-state current must have the same sign as the drag force f.

2.4 Entropy Production in Travelling-Wave–Driven Systems and Current Bounds

A feasible way to verify BASEP current–density relations in a laboratory is to consider an equivalent ring system with the TW external periodic potential $U(x - v_w t)$ and $f = 0$ [62, 71–74]. In such a TW system, the $i^{\rm th}$ component of the probability current vector is

$$J_i^{\rm TW}(\boldsymbol{x},\ t) = \mu\left[-\frac{\partial U(x_i - v_w t)}{\partial x_i} + f_i^{\rm int}(\boldsymbol{x})\right] p_N^{\rm TW}(\boldsymbol{x},\ t) - D\frac{\partial p_N^{\rm TW}(\boldsymbol{x},\ t)}{\partial x_i}. \tag{27}$$

Under a Galilean transformation

$$x_i(t) = x_i^{\rm TW}(t) - v_w t. \tag{28}$$

the TW system maps to the corresponding BASEP with potential $U(x)$ and constant drag force

$$f = -\frac{v_w}{\mu}\,, \tag{29}$$

provided the pair interaction potential $u^{\rm int}(x,\ y)$ is a function of the particle distance $(x - y)$ only. Local densities and currents of the two corresponding systems are related by [56]

$$\varrho^{\rm TW}(x,\ t) = \varrho(x - v_w t,\ t), \tag{30}$$

$$j^{\rm TW}(x,\ t) = v_w \varrho(x - v_w t,\ t) + j(x - v_w t,\ t)\,. \tag{31}$$

A remarkable aspect of this mapping that has not been discussed in our previous work relates to the fundamental difference of dissipations (their physical origins and their values) in the two pictures. In fact, hopping events that contribute positively to the dissipation (total entropy production) in one picture cause a decrease of the dissipation in the other.

In the BASEP, the dissipation equals the average work done by a constant nonconservative force on all the particles; see (26). In the TW system, there is no nonconservative force. Instead, each particle is acted upon by the time-dependent force $[-U'(x - v_w t)]$, and the sum of these actions over all particles gives the total power input into the system. In the steady state, this power is dissipated into the ambient heat bath via friction. Therefore, in the TW model, the total entropy production averaged over one period $\tau = v_{\rm w}/\lambda$ reads (the bar denoting period-averaging

in time)

$$\overline{\dot{S}_{\mathrm{tot}}^{\mathrm{TW}}} = -\frac{1}{T}\sum_{i=1}^{N}\frac{1}{\tau}\int_0^\tau \mathrm{d}t\left\langle\frac{\partial U(x_i - v_w t)}{\partial t}\right\rangle. \tag{32}$$

After some algebra similar to that in Section 2.3, one obtains [56]

$$\overline{\dot{S}_{\mathrm{tot}}^{\mathrm{TW}}} = \frac{v_w \overline{j_{\mathrm{ss}}^{\mathrm{TW}}}}{\mu T} L \geq 0, \tag{33}$$

which means that the period-averaged stationary current $\overline{j_{\mathrm{st}}^{\mathrm{TW}}}$ must have the same sign as v_w. Hence, there are no current reversals in a TW system.

Furthermore, we can relate the TW current in (33) to the corresponding BASEP by taking the period-averaged form of (31) in the steady state:

$$\overline{\dot{S}_{\mathrm{tot}}^{\mathrm{TW}}} = \frac{v_w^2\rho + v_w j_{\mathrm{ss}}}{\mu T} L \geq 0. \tag{34}$$

Here, the two terms in the numerator have clear physical meanings. The first contains the expression v_w^2/μ equal to the dissipated power by a particle moving at constant velocity v_w in the fluid characterised by the friction coefficient $1/\mu$. This term gives the maximal possible dissipation in the TW system corresponding to the case with no jumps over potential barriers where the motion of each particle is exactly phase-locked with the TW potential $U(x - v_w t)$. The second term contains the current in the corresponding BASEP and is negative because v_w and f have opposite signs. Recalling (29), we see that the second term equals exactly the dissipation in the BASEP (26) up to the minus sign. It tells us that the total TW dissipation is diminished by the difference of the average number of jumps over potential barriers in and against bias direction.

Overall, the inequality in (34) implies

$$0 \leq j_{\mathrm{ss}}(\rho,\ \sigma) \leq \mu f \rho, \tag{35}$$

for $f > 0$; that is, we obtain the upper bound $\mu f \rho$ for the current, whereas the lower bound follows from (26) as already discussed.

3 Hardcore Interacting Particles in Harmonic Potential

The paradigmatic variant of the BASEP with hardcore-interacting particles diffusing in the external harmonic potential

$$U(x) = \frac{U_0}{2}\cos\left(\frac{2\pi x}{\lambda}\right) \tag{36}$$

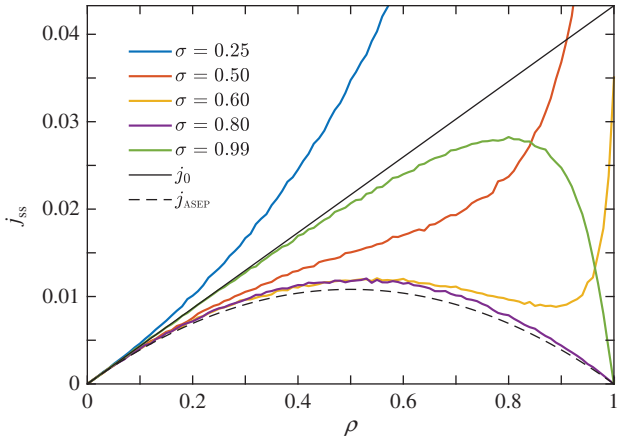

Figure 1: Simulated steady-state current j_{ss} in the BASEP with cosine potential (36) as a function of the density ρ for different particle sizes σ. The solid black line marks the current of noninteracting particles $j_0(\rho) = v_0\rho$; and the dashed line, the current–density relation $j_{\mathrm{ASEP}}(\rho) = v_0\rho(1-\rho)$ of a corresponding ASEP [$v_0 = 0.043$ from (37)].

has been studied thoroughly in our previous works [55, 56, 63]. Here, we review its basic properties that shall serve as a "reference case" for the following analysis.

In all illustrations, we fix units setting $\lambda = 1$ (defines units of length), $\lambda^2/D = 1$ (time), $k_{\mathrm{B}}T = 1$ (energy); this implies that $\mu = D/(k_{\mathrm{B}}T) = 1$ also. We assume $U_0 \gg 1$, which leads to a hopping-like motion between potential wells that resembles the dynamics on a lattice.

Four representative shapes of current–density relations are shown in Figure 1. In the low-density limit, all curves collapse to the linear behaviour $j_0(\rho) = v_0\rho$ with the slope given by the velocity v_0 of a single (noninteracting) particle. This is given by [75]

$$v_0 = \frac{D\lambda(1 - e^{-\beta f\lambda})}{\int_0^\lambda \mathrm{d}x \int_x^{x+\lambda}\mathrm{d}y\ \exp[\beta(U(y) - fy - U(x) + fx)]}, \tag{37}$$

where $\beta = 1/(k_{\mathrm{B}}T)$. Beyond the small-$\rho$ region, the shapes change strongly with the particle size σ. This complex behaviour is caused by three competing collective effects:

(i) The *barrier reduction effect* leads to a current increase with ρ. It appears in multioccupied wells, where particles are pushing each other to regions of higher potential energy and thus decrease an effective barrier for a transition to neighbouring wells. The effect is best visible for small σ causing currents to be larger than $j_0(\rho) = v_0\rho$ (solid black line in Fig. 1). Likewise, for small and moderate σ, the

strong current increase at larger ρ is due to the occurrence of double-occupied wells.

(ii) The *blocking effect* suppresses the current by reducing the number of transitions between neighbouring wells. It occurs for larger particle sizes: an extended particle is more easily blocked by another one occupying the neighbouring well (compared to smaller σ). To contrast with the most extreme case of blocking, the parabolic current–density relations $j_{\mathrm{ASEP}}(\rho) = v_0\rho(1-\rho)$ of a corresponding ASEP is shown as the dashed line in Figure 1.

(iii) The *exchange symmetry effect* causes a deformation of the current–density relation towards the linear behaviour $j_0(\rho) = v_0\rho$ if the particle size is close to $\sigma = m$, $m = 0,\ 1,\ 2,\ \ldots$, that is, a multiple integer of λ. In the commensurate case $\sigma = m$, the current of interacting particles becomes equal to that of noninteracting ones. This effect is a consequence of the general relation

$$j_{\mathrm{ss}}(\rho,\ \sigma) = (1-m\rho)\, j_{\mathrm{ss}}\left(\frac{\rho}{1-m\rho},\ \sigma - m\lambda\right) \tag{38}$$

that maps the stationary current in a system with particles of diameter σ and density ρ to that with particles of diameter $\sigma - m\lambda$ and density $\rho/(1-m\rho)$, where $m = \mathrm{int}(\sigma/\lambda)$ is the integer part of σ/λ.

4 Impact of External Periodic Potential

As discussed in the Introduction, we consider further external potentials, namely, the Kronig–Penney, a piecewise linear, and a triple-well potential. These potentials are plotted in Figure 2b–d together with the cosine potential of our reference system in Figure 2a.

4.1 Kronig–Penney Potential

The Kronig–Penney potential has the form

$$U(x) = \begin{cases} 0\,, & 0 \le x < \lambda_{\mathrm{w}}\,, \\ U_0\,, & \lambda_{\mathrm{w}} \le x < \lambda\,, \end{cases} \tag{39}$$

where λ_{w} is width of the rectangular well, and $\lambda_{\mathrm{b}} = \lambda - \lambda_{\mathrm{w}}$ is the width of the rectangular barrier. We are interested in the current–density relation for different λ_{w} in the limit of large $U_0 \gg 1$. Specifically, we take the same value $U_0 = 6$ as for the reference BASEP with cosine potential discussed in Section 3. In particular, we aim to clarify whether a current enhancement over that of noninteracting particles still occurs. As all particles dragged from one well to a neighbouring one have to surmount the same barrier height U_0 now, it is not clear whether multiple occupations of wells lead to an effective barrier reduction. The blocking and exchange symmetry effect are expected to influence the current in an analogous manner.

Inserting the Kronig–Penney potential in (37) yields

$$v_0(\lambda_{\mathrm{w}}) = \frac{A}{B} \tag{40a}$$

$$A = \frac{D}{\lambda}(\beta f\lambda)^2(e^{\beta f\lambda} - 1) \tag{40b}$$

$$B = 2[e^{\beta f\lambda_{\mathrm{w}}} + e^{\beta f(\lambda-\lambda_{\mathrm{w}})} - e^{\beta f\lambda} - 1] \times [1 - \cosh(\beta U_0)] + \beta f\lambda(e^{\beta f\lambda} - 1) \tag{40c}$$

for the single-particle velocity. This result is plotted in Figure 3. As expected, $v_0(\lambda_{\mathrm{w}})$ approaches the mean drift velocity μf of a single particle in a flat potential in the limits $\lambda_{\mathrm{w}} \to 0$ (zero well width) and $\lambda_{\mathrm{w}} \to 1$ (zero barrier width). With increasing width of the wells (or of the barriers), $v_0(\lambda_{\mathrm{w}})$ rapidly decreases. Interestingly, (40c) implies the symmetry $v_0(\lambda_{\mathrm{w}}) = v_0(1-\lambda_{\mathrm{w}}) = v_0(\lambda_{\mathrm{b}})$, which means the single-particle velocity remains unaltered if the barriers and wells are interchanged.

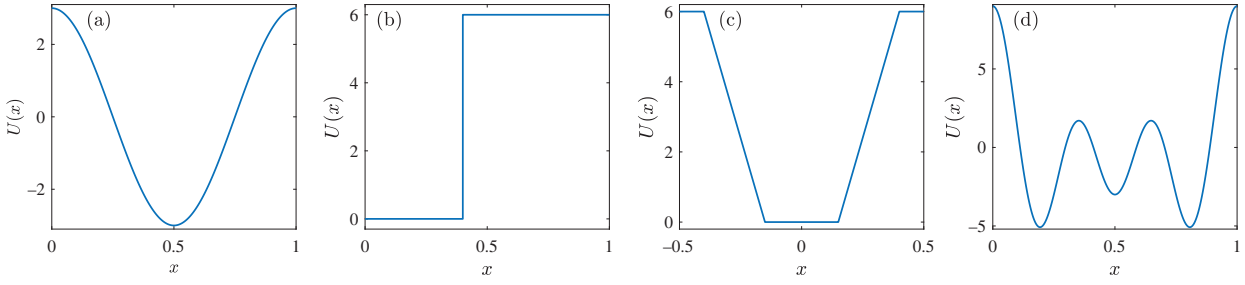

Figure 2: The different periodic externals potentials investigated for comparing current–density relations: (a) cosine (36), (b) Kronig–Penney (39), (c) piecewise linear (42), and (d) triple-well (43).

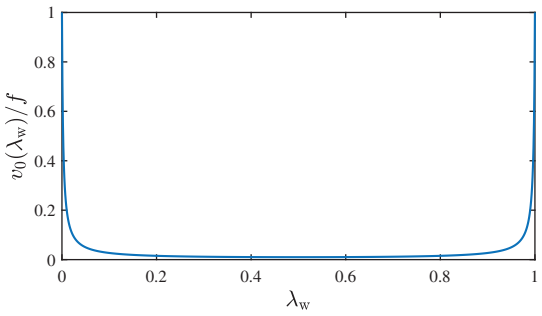

Figure 3: Drift velocity of a single particle in dependence of λ_w for the Kronig–Penney potential in (39); the velocity is normalised to f, i.e. its value in a flat (vanishing) external potential. The barrier height and drag force are $U_0 = 6$ and $f = 0.2$.

Current–density relations for hardcore-interacting particles calculated from the SDA (cf. Section 2.2) are shown in Figure 4 for five different values of λ_w. For each λ_w, we plotted j_{ss}/v_0 vs. ρ for eight rod lengths σ analogous to our representation of current–density curves in Figure 1. As can be seen from the graphs, the shapes of the current–density relation are qualitatively comparable to that in Figure 1 for all λ_w, as well as their overall change with the diameter σ. This means that the interplay of the barrier reduction, blocking, and exchange symmetry is still present. As expected, the overall strengths of the effects in modifying the current of noninteracting particles become weaker with increasing λ_w; for $\lambda_w \to 1$, the current $j_{ss}(\rho,\ \lambda_w)$ indeed approaches $j_0(\rho,\ \lambda_w \to 1) = \rho v_0(\lambda_w \to 1) = \mu f \rho$.

The barrier reduction, however, can no longer be associated with a decrease of an effective barrier height, when two or more particles occupy a potential well. For the Kronig–Penney potential in (39), all particles in a multiple-occupied well have zero energy and need to overcome U_0. Nevertheless, we can attribute the enhancement of the current compared to that of noninteracting particles with a barrier reduction. To see this, we analyse the potential of mean force

$$U_{mf}(x) = k_B T \ln \varrho_{eq}(x) + C = U_{mf}(x + \lambda) \qquad (41)$$

for both the cosine and the Kronig–Penney potential, where the constant C is chosen to give a potential minimum equal to zero. If considering driven Brownian motion of noninteracting particles in the potential $U_{mf}(x)$, the current in the linear response limit would be equal to the many-particle current in the SDA. We therefore can interpret U_{mf} as an effective barrier in the many-particle system. In Figure 5, we show U_{mf}/U_0 for both the cosine and the Kronig–Penney potential. At the maximum of the cosine

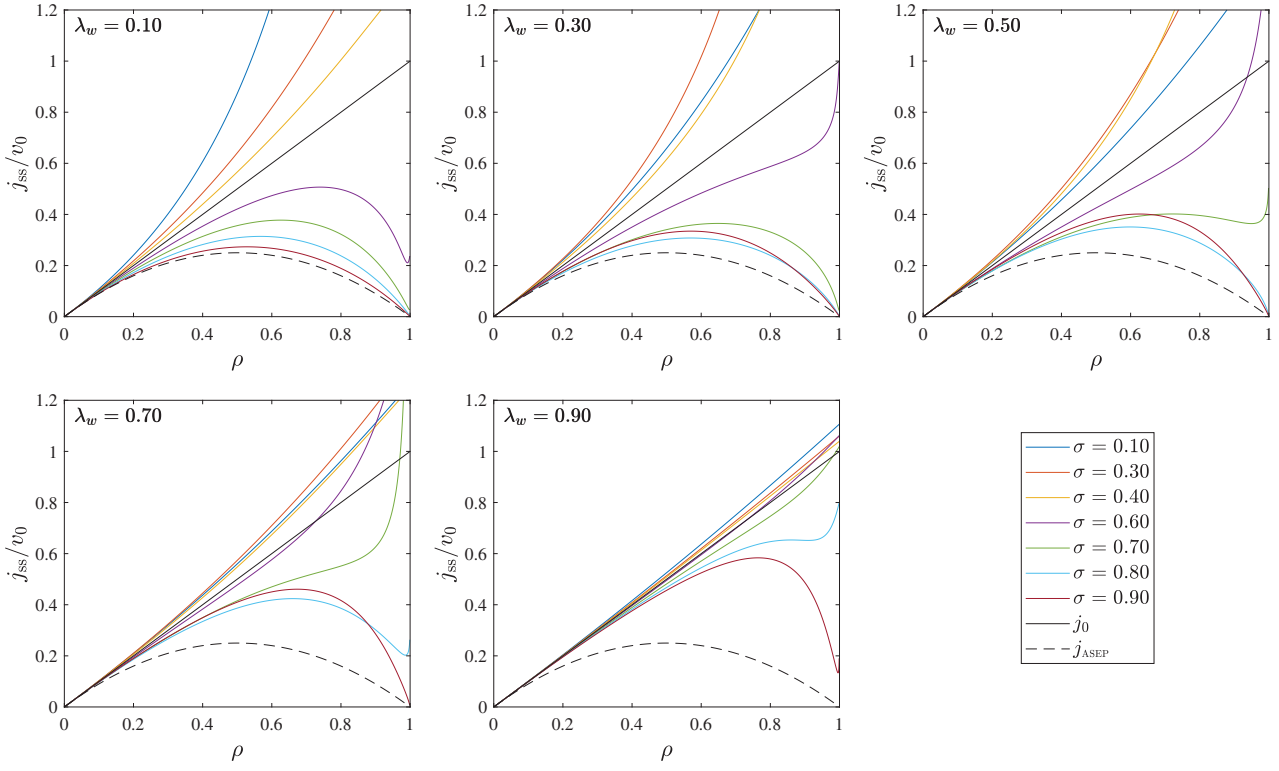

Figure 4: Current j_{ss}, normalised with respect to $v_0(\lambda_w)$ (Fig. 3), for the Kronig–Penney potential in the small-driving approximation as a function of ρ for different σ and (a) $\lambda_w = 0.1$, (b) 0.3, (c) 0.5, (d) 0.7, and (e) 0.9. The barrier height is $U_0 = 6$.

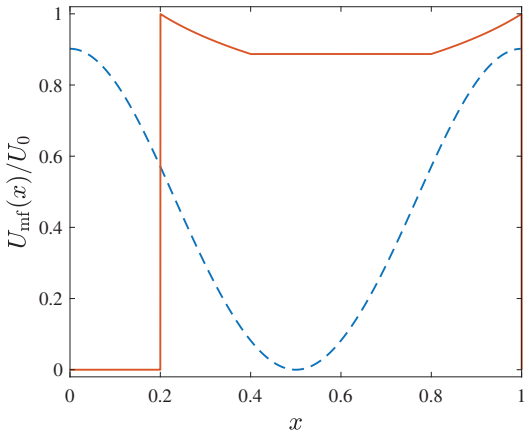

Figure 5: Potential of mean force U_{mf} for the cosine potential (blue dashed line) and the Kronig–Penney potential with $\lambda_{\mathrm{w}} = 0.2$ (solid red line). Parameters are $\sigma = 0.2$, $\rho = 0.5$, and $U_0 = 6$ for both potentials.

potential at $x = 0$, we find $U_{\mathrm{mf}}/U_0 < 1$, which means the barrier height is reduced. In contrast, the barrier at the step of the Kronig–Penney potential equals U_0 ($U_{\mathrm{mf}}(x = \lambda_{\mathrm{w}})/U_0 = 1$ in Figure 5). However, a barrier reduction is now clearly seen in the plateau part of the barrier in the range $\lambda_{\mathrm{w}} < x < 1$. We thus can distinguish between two types of barrier reduction, namely, the first type associated with a reduction of the barrier height and the second type associated with a lowering of the barrier plateau.

Generally, a single-well periodic potential can be characterised roughly by the widths of a valley and barrier part and the flanks in between these parts. A simple representation is given by the piecewise linear potential

$$U(x) = \begin{cases} 0\,, & 0 \le |x| \le \dfrac{\lambda_{\mathrm{w}}}{2}\,, \\ \dfrac{U_0}{\lambda_{\mathrm{f}}}\left(|x| - \dfrac{\lambda_{\mathrm{w}}}{2}\right), & \dfrac{\lambda_{\mathrm{w}}}{2} \le |x| \le \dfrac{\lambda_{\mathrm{w}}}{2} + \lambda_{\mathrm{f}}\,, \\ U_0\,, & \dfrac{\lambda_{\mathrm{w}}}{2} + \lambda_{\mathrm{f}} \le |x| \le \lambda\,, \end{cases} \tag{42}$$

shown in Figure 2c, where λ_{w}, λ_{f}, and $\lambda_{\mathrm{b}} = \lambda - \lambda_{\mathrm{w}} - 2\lambda_{\mathrm{f}}$ are specifying the widths of the valley, barrier, and flanks. We performed additional calculations in the SDA for this potential. For various fixed λ_{w} and λ_{f}, we always found current–density relations with a behaviour similar to that found in Figure 1 for the BASEP with cosine potential. This model may thus be viewed as representative for Brownian single-file transport through single-well periodic potentials with barriers much larger than the thermal energy.

Current–density relations with different characteristics can, however, be obtained for multiple-well periodic potentials, as we discuss next.

4.2 Triple-Well Potential

The triple-well potential shown in Figure 2d is

$$U(x) = U_0 \sum_{j=1}^{3} (j+1) \cos\left(\frac{2\pi j x}{\lambda}\right), \tag{43}$$

where we choose $U_0 = 1$ here. For this potential, our calculations of $j_{\mathrm{ss}}(\rho)$ based on the SDA show a very sensitive dependence on σ. We concentrate here on one particle diameter $\sigma = 0.323$, where several local extrema occur; see Figure 6. In this figure, currents are shown up to a density (filling factor) $N/M = \rho = 2.98$, corresponding to a coverage $\rho\sigma \cong 96\%$ of the system by the hard rods. If ρ approaches its maximal value $1/\sigma \cong 3.10$ corresponding to a complete coverage, the numerical calculation of the equilibrium density profile from (19) becomes increasingly difficult. Hence, we refrained to show current data for $\rho > 2.98$ due to a lack of sufficient numerical accuracy when calculating $\varrho_{\mathrm{eq}}(x)$. It is important to state in this context that the current for $\rho \to 1/\sigma$ is expected to approach that of noninteracting particles in a flat potential [56]; that is, it should hold $j_{\mathrm{ss}}(\rho,\ \sigma) \sim \mu f \rho$ for $\rho \to 1/\sigma$ (except for the singular point $\rho = 1/\sigma$, where $j_{\mathrm{ss}}(1/\sigma,\ \sigma) = 0$). This means that the current in Figure 6 must steeply rise for $\rho \to 1/\sigma$; that is, there must appear a further local minimum for $\rho > 2.98$. These arguments apply also to the currents shown in Figures 1 and 4.

To explain the occurrence of the local extrema in Figure 6, we resort to (15) with $\chi = 0$, that is, the SDA. This equation can be interpreted by considering $\mu\varrho_{\mathrm{eq}}(x)\mathrm{d}x/\lambda$ to be the "local conductivity" of a line segment dx. A serial connection of these segments implies that the "total

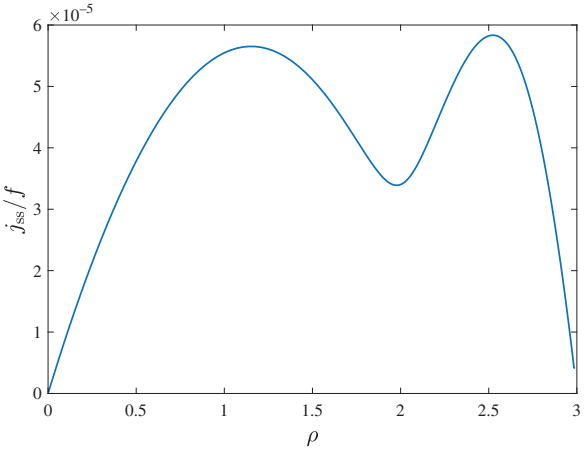

Figure 6: Current j_{ss}, normalised with respect to f, for the triple-well potential in the small-driving approximation as a function of ρ for $\sigma = 0.323$. Densities at the local maxima are $\rho_{\mathrm{max},\,1} = 1.14$ and $\rho_{\mathrm{max},\,2} = 2.53$, and $\rho_{\mathrm{min}} = 1.98$ at the local minimum.

conductivity" is given by the inverse of the sum of the inverse local conductivities, corresponding to a summation of the respective "local resistivities." A stronger localisation of $\rho_{\mathrm{eq}}(x)$ around the minima of the potential leads to a smaller conductivity and hence a smaller current $j_{\mathrm{ss}}(\rho)$, whereas less localised density profiles lead to larger $j_{\mathrm{ss}}(\rho)$.

Using this picture, the occurrence of the first maximum in $j_{\mathrm{ss}}(\rho)$ can be traced back to an increasing occurrence of double-occupied wells for $\rho \gtrsim 1$. In double-occupied wells, particle motion is more restricted, leading to a stronger particle localisation at the two deeper minima at about $x \simeq 0.2$ and $x \simeq 0.8$; see Figure 2d. Accordingly, $j_{\mathrm{ss}}(\rho)$ starts to decrease with ρ for $\rho \gtrsim 1$ ($\rho_{\mathrm{max},\,1} \cong 1.14$ in Fig. 6). The decrease of $j_{\mathrm{ss}}(\rho)$ continues up to a filling factor of about two ($\rho_{\mathrm{min}} \cong 1.98$ in Fig. 6), above which more than two particles occupy a well on average. With a significant appearance of triple-occupied wells goes along first a stronger spreading of the density, as the minimum of the potential at $x = 1/2$ becomes occupied in wells containing three particles. The spreading of the density causes $j_{\mathrm{ss}}(\rho)$ to increase for $\rho \gtrsim 2$. A counteracting effect, however, is a strong particle localisation at all potential minima in neighbouring triple-occupied wells, where the hardcore constraints force the particles to become strongly localised around the potential minima. For $\rho \gtrsim 2.5$ ($\rho_{\mathrm{max},\,2} \cong 2.53$ in Fig. 6), every second well is occupied by three particles on average, which lets $j_{\mathrm{ss}}(\rho)$ decrease again with further increasing ρ.

The more complex current–density relation in Figure 6 leads to a richer variety of NESS phases in open systems compared to the reference BASEP, which can exhibit up to five different phases [55, 56]. To identify all possible NESS phases, we consider the particle exchange with two reservoirs L and R at the left and right ends of an open system to be controlled by two parameters ρ_{L} and ρ_{R}. As discussed in connection with (1) in the Introduction, these control parameters can be considered as effective densities, or they can be associated with true reservoir densities for specific bulk-adapted couplings of the system to the reservoirs [33, 34].

Applying (1) with $\rho_- = \rho_{\mathrm{L}}$ and $\rho_+ = \rho_{\mathrm{R}}$ to the current–density relation in Figure 6 results in the diagram with seven different NESS phases I–VII shown in Figure 7. The colour coding shows the value of the bulk density ρ_{b}, that is, the order parameter of the phase transitions. Solid lines mark first-order, and dashed lines mark second-order phase transitions, which is reflected in the smooth (continuous) or sudden (jump-like) changes of the colour. The seven phases can be classified in two categories: boundary-matching phases, where ρ_{b} is equal to either ρ_{L} or ρ_{R}, and extremal current phases, where ρ_{b} is

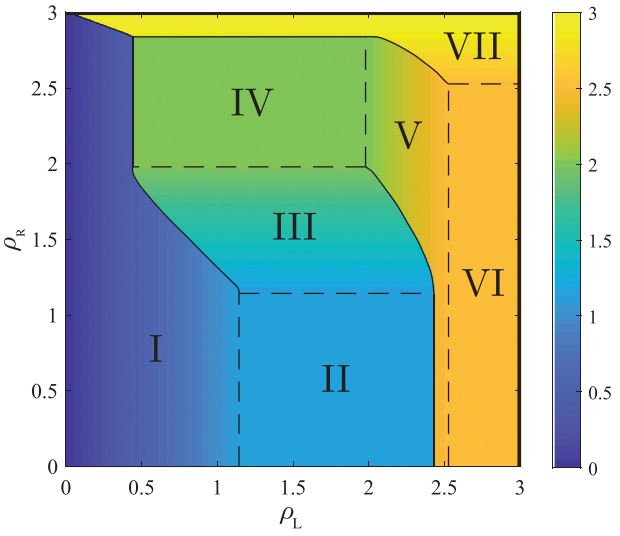

Figure 7: Phase diagram of NESS for the triple-well potential obtained by applying the extremal current principles to the current–density relation in Figure 6. The colour bar encodes the values of the bulk density ρ_{b} in an open system coupled to particle reservoirs. Phases I and V are left-boundary matching phases with $\rho_{\mathrm{b}} = \rho_{\mathrm{L}}$, phases III and VII are right-boundary matching phases with $\rho_{\mathrm{b}} = \rho_{\mathrm{R}}$, phases II and VI are maximal current phases with $\rho_{\mathrm{b}} = \rho_{\mathrm{max},\,1}$ and $\rho_{\mathrm{b}} = \rho_{\mathrm{max},\,2}$, respectively, and phase IV is a minimal current phase with $\rho_{\mathrm{b}} = \rho_{\mathrm{min}}$. Solid (dashed) lines mark first-(second-)order phase transitions. The dark black bars at the boundaries mark the two stripes $2.98 < \rho_{\mathrm{L,R}} \leq 1/\sigma \cong 3.1$, where additional phases appear (see the discussion in Section 4.2, Triple-Well Potential).

equal to one of the densities at which $j_{\mathrm{ss}}(\rho)$ has a local extremum in Figure 6. Specifically, phases I and V are left-boundary matching phases with $\rho_{\mathrm{b}} = \rho_{\mathrm{L}}$, phases III and VII are right-boundary matching phases with $\rho_{\mathrm{b}} = \rho_{\mathrm{R}}$, phase II is a maximal current phase with $\rho_{\mathrm{b}} = \rho_{\mathrm{max},\,1}$, phase VI is a maximal current phase with $\rho_{\mathrm{b}} = \rho_{\mathrm{max},\,2}$, and phase IV is a minimal current phase with $\rho_{\mathrm{b}} = \rho_{\mathrm{min}}$. If one takes into account the existence of the further minimum for $\rho > 2.98$ in the current–density relation (see discussion above), then even more phases are possible. These additional phases, however, must appear in the two stripes $2.98 < \rho_{\mathrm{L,\,R}} \leq 1/\sigma \cong 3.1$, that is, in a very narrow range of one of the two control parameters (marked in black in Fig. 7).

5 Impact of Interactions Other Than Hardcore Exclusions

In this section, we investigate the impact of other particle interactions beyond hardcore exclusion for the cosine external potential in (36). This is done in two

different settings. First, we investigate the repulsive Yukawa potential

$$u_Y^{\text{int}}(r) = A_Y \frac{e^{-r/\xi}}{r/\xi}, \tag{44}$$

between particles at distance r for a fixed small amplitude $A_Y = 1$ and different decay lengths ξ. Second, we combine this Yukawa interaction with hardcore interactions. For obtaining current–density relations, we here employ Brownian dynamics simulations. This is because an exact density functional is not available for the Yukawa interaction, and the SDA with a precise determination of $\varrho_{\text{eq}}(x)$ cannot be applied. For performing the Brownian dynamics simulations, we used a standard Euler integration scheme of the Langevin equations (2) with a time step $\Delta t = 10^{-4}$. To deal with the hardcore interactions, the algorithm developed in [76] was applied.

Current–density relations for the Yukawa potential without additional hardcore interactions are shown in Figure 8 for six different values of ξ. These may be viewed to resemble effective particle diameters σ of hardcore-interacting systems. For small ξ, that is, $\xi = 0.166$ and 0.333 in Figure 8, j_{ss} shows an enhancement over that of noninteracting particles (solid black line) due to a prevailing barrier reduction effect similar to that in the reference BASEP for small σ. When enlarging ξ, the current is reduced for small ρ compared to that of noninteracting particles, while it rises strongly for large ρ. Again, this behaviour is analogous to that in the reference BASEP for increasing σ. Because the (effective) blocking effect is not so strong for $A_Y = 1$, the current–density curves do not approach the limiting $j_{\text{ASEP}}(\rho)$ as closely as for hardcore interactions. Nevertheless, one can say that the change of the current–density relation with varying ξ is reflecting the interplay of a barrier reduction and blocking effect as in the reference BASEP.

However, one cannot find certain ξ values, where the current–density relation equals that of noninteracting particles for all ρ. The peculiar exchange symmetry effect in the BASEP for commensurate $\sigma = m$, $m = 0,\ 1,\ 2\ldots$, is caused by the invariance of the stochastic particle dynamics against a specific coordinate transformation containing σ [55, 56]. Such coordinate transformation does not exist for the Yukawa potential.

For the Yukawa potential with additional hardcore interactions, we found changes of current–density curves caused by the barrier reduction and blocking effect as discussed above. But it is interesting to analyse now whether the relation $j_{\text{ss}}(\rho) = j_0(\rho) = v_0\rho$ for commensurate $\sigma = m$ and $\xi = 0$ is approximately reflected in current–density relations for $\xi > 0$, where the exchange symmetry effect is no longer strictly valid. One may expect that the hardcore-interacting system should be only weakly perturbed by the Yukawa potential if A_Y is of the order of the thermal energy and ξ not too large compared to σ. This is indeed confirmed by simulation results for $\sigma = 1$ shown in Figure 9. The data points for $\xi = 0.166$ and $\xi = 0.333$ lie almost directly on the curve $j_0(\rho)$ up to the highest simulated density $\rho = 0.9$. With increasing ξ, deviations from the linear

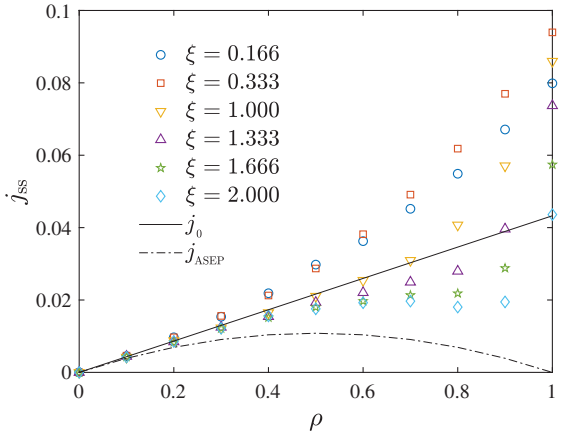

Figure 8: Simulated current–density relations for the external cosine potential (36) and particle interactions given by the Yukawa potential in (44). The amplitude of the Yukawa potential is $A_Y = 1$, and ξ values specify different decay lengths. The other simulation parameters are $U_0 = 6$ and $f = 2$. The solid line marks the current $j_0(\rho) = v_0\rho$ for noninteracting particles, and the dashed line indicates the current–density relation $j_{\text{ASEP}}(\rho) = v_0\rho(1-\rho)$ of a corresponding ASEP (same curves as in Fig. 1).

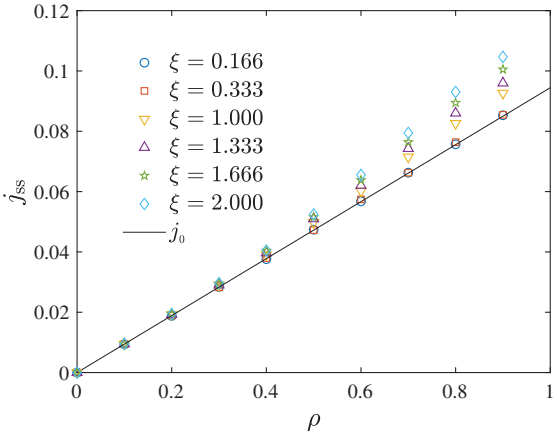

Figure 9: Simulated current–density relations for the cosine external potential and Yukawa interactions as in Figure 8, and additional hardcore interactions for commensurate particle size $\sigma = 1$. Parameters for the drag force, as well as for the amplitudes of the cosine and Yukawa potential, are chosen as in Figure 8. The solid line marks the current $j_0(\rho) = v_0\rho$ for noninteracting particles (same line as in Figs. 1 and 8).

behaviour are seen, which become the more pronounced the larger ρ. But even for $\xi = 2$, $j_{ss}(\rho)$ follows $j_0(\rho)$ closely up to $\rho = 0.4$. We thus conclude that slight deviations from a perfect hardcore interaction, as they are always present in experiments, still allow an identification of the exchange symmetry effect.

6 Summary and Conclusions

To analyse how generic our previous findings are for the nonequilibrium physics of the BASEP in a sinusoidal potential, we have studied the driven Brownian motion of hardcore-interacting particles for other external periodic potentials. Our calculations were carried out based on a small-driving approximation, which refers to the linear response under neglect of a period-averaged mean interaction force. If the external periodic potential exhibits a single-well structure between barriers, that is, if there is only one local minimum per period, our results provide evidence that the various characteristic shapes of bulk current–density relations $j_{ss}(\rho)$ for different particle sizes σ are always occurring. There are differences in the exact functional form and at which σ the type of shape is changing. For all single-well periodic potentials, it is the interplay of a barrier reduction, blocking, and exchange symmetry effect that causes a particular shape to appear. Even for a Kronig–Penney potential with alternating rectangular well and barrier parts, where the barrier reduction effect is not so obvious, we showed that an enhancement of the current over that of noninteracting particles occurs. For that potential, this enhancement can be attributed to an effective reduction of the barrier plateau parts. The generic behaviour of the bulk current–density relations implies that for single-well periodic potentials up to five different NESS phases appear in open BASEP systems coupled to particle reservoirs. This can be concluded by applying the extremal current principles [27, 29].

More complex shapes of $j_{ss}(\rho)$ can occur in multiple-well periodic potentials. This was demonstrated for a particular triple-well potential, where our calculations yielded a current–density relation with two local maxima for a certain particle size. In that case, the extremal current principles predict more than five different NESS phases in an open system. When neglecting a narrow range of very high effective reservoir densities, which would be very difficult to realise by specific system-reservoir couplings in simulations or experiments, up to seven different NESS phases are possible. We point out that these results were obtained here for demonstration purposes. Systematic investigations of multiple-well external potentials should be performed in the future with a goal to reach a general classification similar as for the BASEP for single-well periodic potentials.

Current–density relations with several local maxima are particularly interesting in the case of "degenerate maxima," that is, when the current at the maxima has the same value. In such situations, coexisting NESS phases of maximal current can occur in a whole connected region of the space spanned by the parameters controlling the coupling to the environment [77]. Such states of coexisting extremal current phases have not yet been studied in detail in the literature. Preliminary results for driven lattice gases indicate that fluctuations of interfaces separating extremal current phases exhibit an anomalous scaling with time and system length.[2] This is in contrast to the already well-studied interface fluctuations between the low- and high-density phases in the ASEP, which at long times show a simple random-walk behaviour.

We furthermore performed Brownian dynamics simulations of driven single-file diffusion through a cosine potential for a repulsive particle interaction other than hardcore exclusion. Specifically, we chose a Yukawa interaction with a small interaction amplitude equal to the thermal energy and studied the behaviour for different decay lengths ξ. Current–density relations for this system showed similar shapes as for the BASEP except for the effects implied by the exchange symmetry effect, which is absent for other interactions than hardcore. The change of shapes is solely determined by the interplay of a barrier reduction and effective blocking effect. If the hardcore interaction and the weak Yukawa interaction are combined, the consequences of the exchange symmetry effect can still be seen for particle sizes commensurate with the wavelength of the cosine potential. The current $j_{ss}(\rho)$ follows closely that of noninteracting particles up to high densities even for large ξ. This means that deviations from a perfect hardcore interaction in experiments should still allow one to verify the exchange symmetry.

Acknowledgements: Financial support by the Czech Science Foundation (Funder Id: http://dx.doi.org/10.13039/501100001824, project no. 20-24748J) and the Deutsche Forschungsgemeinschaft (Funder Id: http://dx.doi.org/10.13039/501100001659, project no. 397157593) is gratefully acknowledged. We sincerely thank the members of the DFG Research Unit FOR 2692 for fruitful discussions.

2 D. Locher, bachelor thesis (in German), Osnabrück University (2018); M. Bosi, D. Locher, and P. Maass, to be published.

Appendix: Example for Connection of ASEP to Quantum Spin Chain

Let $p(n, t)$ denote the probability of configurations $n = \{n_i,\ i = 1,\ \ldots,\ L\}$ of occupation numbers $n_i \in \{0,\ 1\}$ in a single-species fermionic lattice gas at time t. Its time evolution is described by the master equation

$$\frac{\mathrm{d}p(n,\ t)}{\mathrm{d}t} = \sum_{n'}[w_{nn'}p(n',\ t) - w_{n'n}p(n,\ t)] = \sum_{n'} H_{nn'}p(n',\ t) \tag{A.1}$$

where $w_{nn'}$ is the transition rate from configuration n' to n (for $n' \neq n$; otherwise, $w_{nn} = 0$), and $H_{nn'} = w_{nn'} - \delta_{nn'}\sum_{n''} w_{n''n}$. This master equation corresponds to the occupation number representation of a Schrödinger equation

$$\frac{\mathrm{d}|p\rangle}{\mathrm{d}t} = H|p\rangle \tag{A.2}$$

in imaginary time [3, 4].

For the ASEP with periodic boundary conditions ($n_{L+1} = n_1,\ n_0 = n_L$), the transitions rates $w_{nn'}$ can be written as

$$w_{nn'} = \sum_{j=1}^{L} \delta_{n'n^{(j)}}[\Gamma_- n'_{j+1}(1 - n'_j) + \Gamma_+ n'_j(1 - n'_{j+1})] = \sum_{j=1}^{L} \delta_{n'n^{(j)}}[\Gamma_-(1 - n_{j+1})n_j + \Gamma_+(1 - n_j)n_{j+1}]\,, \tag{A.3}$$

where $n^{(j)}$ denotes the configuration n with the occupation numbers at sites j and $(j+1)$ interchanged, i.e. $n_k^{(j)} = n_k$ for $k \neq j,\ (j+1)$, $n_j^{(j)} = n_{j+1}$, and $n_{j+1}^{(j)} = n_j$. Accordingly, the matrix elements $H_{nn'} = \langle n|H|n'\rangle = w_{nn'} - \delta_{nn'}\sum_{n''} w_{n''n}$ are

$$H_{nn'} = \sum_{j=1}^{L}\{\delta_{n'n^{(j)}}[\Gamma_- n_j(1 - n_{j+1}) + \Gamma_+(1 - n_j)n_{j+1}] - \delta_{nn'}[\Gamma_-(1 - n_j)n_{j+1} + \Gamma_+ n_j(1 - n_{j+1})]\}. \tag{A.4}$$

Because $\langle n|c_j^\dagger c_{j+1}|n'\rangle = \delta_{n'n^{(j)}} n_j(1-n_{j+1})$ for creation and annihilation operators $c_j^\dagger$ and c_j of a particle at site j, the matrix elements in (A.4) are equal to those of the Hamiltonian

$$H = \sum_{j=1}^{L}\{\Gamma_-[c_j^\dagger c_{j+1} - n_{j+1}(1 - n_j)] + \Gamma_+[c_{j+1}^\dagger c_j - n_j(1 - n_{j+1})]\} \tag{A.5}$$

of spinless fermions, which for $\Gamma_+ \neq \Gamma_-$ is non-Hermitian. In a representation by Pauli matrices, one can write $c_j^\dagger = \sigma_j^+/2 = (\sigma_j^x + i\sigma_j^y)/2$, $c_j = \sigma_j^-/2 = (\sigma_j^x - i\sigma_j^y)/2$, and $n_j = (1 + \sigma_j^z)/2$, giving

$$H = \frac{1}{4}\sum_{j=1}^{L}[\Gamma_-\sigma_j^+\sigma_{j+1}^- + \Gamma_+\sigma_{j+1}^+\sigma_j^- + (\Gamma_- + \Gamma_+)(\sigma_j^z\sigma_{j+1}^z - 1)]. \tag{A.6}$$

The periodic boundary conditions imply $\sigma_{L+1}^\pm = \sigma_1^\pm$ and $\sigma_{L+1}^z = \sigma_1^z$.

A transformed $H' = VHV^{-1}$ with (nonsingular) operator V has the same spectrum as H, where eigenstates $|\varphi\rangle$ and $|\varphi'\rangle$ of H and H' to the same eigenvalue are related by $|\varphi'\rangle = V|\varphi\rangle$. Such transformation can be used to symmetrise the non-Hermitian part $(\Gamma_-\sigma_j^+\sigma_{j+1}^- + \Gamma_+\sigma_{j+1}^+\sigma_j^-)$ in (A.6) by choosing $V = \exp(\alpha\sum_{j=1}^{L} j\sigma_j^z)$ with some constant α, because $V\sigma_j^\pm V^{-1} = e^{\pm 2\alpha j}\sigma_j^\pm$ [6]. With $V\sigma_j^+\sigma_{j+1}^-V^{-1} = V\sigma_j^+VV^{-1}\sigma_{j+1}^-V^{-1} = e^{-2\alpha}\sigma_j^+\sigma_{j+1}^-$ and $V\sigma_{j+1}^+\sigma_j^-V^{-1} = e^{2\alpha}\sigma_{j+1}^+\sigma_j^-$, the symmetrisation is achieved by requiring $\Gamma_- e^{-2\alpha} = \Gamma_+ e^{2\alpha}$, that is, by setting $e^\alpha = (\Gamma_-/\Gamma_+)^{1/4}$. The transformed Hamiltonian is that of a quantum *XXZ* chain,

$$H' = \frac{\sqrt{\Gamma_-\Gamma_+}}{2}\sum_{j=1}^{L}(\sigma_j^x\sigma_{j+1}^x + \sigma_j^y\sigma_{j+1}^y + \Delta\,\sigma_j^z\sigma_{j+1}^z - \Delta) \tag{A.7}$$

with $\Delta = (\Gamma_- + \Gamma_+)/(2\sqrt{\Gamma_-\Gamma_+})$, but now non-Hermitian boundary conditions $V\sigma_{L+1}^\pm V^{-1} = V\sigma_1^\pm V^{-1}$, that is, $\sigma_{L+1}^\pm = e^{\mp 2\alpha L}\sigma_1^\pm = (\Gamma_-/\Gamma_+)^{\mp L/2}\sigma_1^\pm$ and $\sigma_{L+1}^z = \sigma_1^z$.

References

[1] B. Derrida, Phys. Rep. **301**, 65 (1998).
[2] G. M. Schütz, in: Phase Transitions and Critical Phenomena, Vol. 19 (Eds. C. Domb, J. Lebowitz), Academic Press, London 2001, p. 1.
[3] L.-H. Gwa and H. Spohn, Phys. Rev. A **46**, 844 (1992).
[4] S. Sandow and S. Trimper, Europhys. Lett. (EPL) **21**, 799 (1993).
[5] S. Sandow, Phys. Rev. E **50**, 2660 (1994).
[6] M. Henkel and G. Schütz, Phys. A **206**, 187 (1994).
[7] R. A. Blythe and M. R. Evans, J. Phys. A Math. Theor. **40**, R333 (2007).
[8] K. Krebs and S. Sandow, J. Phys. A Math. Gen. **30**, 3165 (1997).
[9] B. Derrida and J. L. Lebowitz, Phys. Rev. Lett. **80**, 209 (1998).
[10] B. Derrida, J. L. Lebowitz, and E. R. Speer, Phys. Rev. Lett. **89**, 030601 (2002).
[11] P. L. Krapivsky, K. Mallick, and T. Sadhu, Phys. Rev. Lett. **113**, 078101 (2014).
[12] L. Bertini, A. De Sole, D. Gabrielli, G. Jona-Lasinio, and C. Landim, Rev. Mod. Phys. **87**, 593 (2015).

[13] H. Touchette, Phys. Rep. **478**, 1 (2009).
[14] L. Bertini, A. De Sole, D. Gabrielli, G. Jona-Lasinio, and C. Landim, Phys. Rev. Lett. **94**, 030601 (2005).
[15] T. Bodineau and B. Derrida, Phys. Rev. E **72**, 066110 (2005).
[16] C. Appert-Rolland, B. Derrida, V. Lecomte, and F. van Wijland, Phys. Rev. E **78**, 021122 (2008).
[17] Y. Baek, Y. Kafri, and V. Lecomte, Phys. Rev. Lett. **118**, 030604 (2017).
[18] T. Bodineau and B. Derrida, Phys. Rev. Lett. **92**, 180601 (2004).
[19] G. M. Schütz, J. Stat. Phys. **88**, 427 (1997).
[20] C. A. Tracy and H. Widom, Commun. Math. Phys. **279**, 815 (2008).
[21] C. A. Tracy and H. Widom, J. Stat. Phys. **132**, 291 (2008).
[22] C. A. Tracy and H. Widom, Commun. Math. Phys. **290**, 129 (2009).
[23] K. Johansson, Commun. Math. Phys. **209**, 437 (2000).
[24] M. Kardar, G. Parisi, and Y.-C. Zhang, Phys. Rev. Lett. **56**, 889 (1986).
[25] J. Krug, Phys. Rev. Lett. **67**, 1882 (1991).
[26] G. Schütz and E. Domany, J. Stat. Phys. **72**, 277 (1993).
[27] A. B. Kolomeisky, G. M. Schütz, E. B. Kolomeisky, and J. P. Straley, J. Phys. A Math. Gen. **31**, 6911 (1998).
[28] A. Brzank and G. M. Schütz, J. Stat. Mech. Theor. Exp. **2007**, P08028 (2007).
[29] V. Popkov and G. M. Schütz, Europhys. Lett. **48**, 257 (1999).
[30] J. S. Hager, J. Krug, V. Popkov, and G. M. Schütz, Phys. Rev. E **63**, 056110 (2001).
[31] T. Antal and G. M. Schütz, Phys. Rev. E **62**, 83 (2000).
[32] M. Dierl, P. Maass, and M. Einax, Phys. Rev. Lett. **108**, 060603 (2012).
[33] M. Dierl, M. Einax, and P. Maass, Phys. Rev. E **87**, 062126 (2013).
[34] M. Dierl, W. Dieterich, M. Einax, and P. Maass, Phys. Rev. Lett. **112**, 150601 (2014).
[35] M. R. Evans, EPL **36**, 13 (1996).
[36] R. J. Concannon and R. A. Blythe, Phys. Rev. Lett. **112**, 050603 (2014).
[37] V. Popkov and M. Salerno, Phys. Rev. E **69**, 046103 (2004).
[38] V. Popkov, A. Schadschneider, J. Schmidt, and G. M. Schütz, PNAS **112**, 12645 (2015).
[39] M. Prähofer and H. Spohn, J. Stat. Phys. **115**, 255 (2004).
[40] Z. Chen, J. de Gier, I. Hiki, and T. Sasamoto, Phys. Rev. Lett. **120**, 240601 (2018).
[41] A. Schadschneider, D. Chowdhury, and K. Nishinari, Stochastic Transport in Complex Systems: From Molecules to Vehicles, 3rd ed., Elsevier Science, Amsterdam, 2010.
[42] T. Chou, K. Mallick, and R. K. P. Zia, Rep. Prog. Phys. **74**, 116601 (2011).
[43] C. T. MacDonald, J. H. Gibbs, and A. C. Pipkin, Biopolymers **6**, 1 (1968).
[44] A. B. Kolomeisky, J. Phys. Condens. Matter **25**, 463101 (2013).
[45] C. Appert-Rolland, M. Ebbinghaus, and L. Santen, Phys. Rep. **593**, 1 (2015).
[46] K. Nishinari, Y. Okada, A. Schadschneider, and D. Chowdhury, Phys. Rev. Lett. **95**, 118101 (2005).
[47] C. Appert-Rolland, J. Cividini, and H. J. Hilhorst, J. Stat. Mech. Theor. Exp. **2011**, P10014 (2011).
[48] M. E. Foulaadvand and P. Maass, Phys. Rev. E **94**, 012304 (2016).
[49] B. Hille, Ionic Channels of Excitable Membranes, 3rd ed., Sinauer Associates, Sunderland, MA 2001.
[50] C.-Y. Cheng and C. R. Bowers, ChemPhysChem **8**, 2077 (2007).
[51] M. Dvoyashkin, H. Bhase, N. Mirnazari, S. Vasenkov, and C. R. Bowers, Anal. Chem. **86**, 2200 (2014).
[52] A. Nitzan, Annu. Rev. Phys. Chem. **52**, 681 (2001).
[53] Y. A. Berlin, A. L. Burin, and M. A. Ratner, J. Am. Chem. Soc. **123**, 260 (2001).
[54] H. Risken, The Fokker-Planck Equation: Methods of Solution and Applications, Springer-Verlag, Berlin 1985.
[55] D. Lips, A. Ryabov, and P. Maass, Phys. Rev. Lett. **121**, 160601 (2018).
[56] D. Lips, A. Ryabov, and P. Maass, Phys. Rev. E **100**, 052121 (2019).
[57] A. V. Arzola, M. Villasante-Barahona, K. Volke-Sepúlveda, P. Jákl, and P. Zemánek, Phys. Rev. Lett. **118**, 138002 (2017).
[58] M. J. Skaug, C. Schwemmer, S. Fringes, C. D. Rawlings, and A. W. Knoll, Science **359**, 1505 (2018).
[59] C. Schwemmer, S. Fringes, U. Duerig, Y. K. Ryu, and A. W. Knoll, Phys. Rev. Lett. **121**, 104102 (2018).
[60] R. Stoop, A. Straube, and P. Tierno, Nano Lett. **19**, 433 (2019).
[61] K. Misiunas and U. F. Keyser, Phys. Rev. Lett. **122**, 214501 (2019).
[62] A. V. Straube and P. Tierno, EPL **103**, 28001 (2013).
[63] A. Ryabov, D. Lips, and P. Maass, J. Phys. Chem. C **123**, 5714 (2019).
[64] K. Jain, R. Marathe, A. Chaudhuri, and A. Dhar, Phys. Rev. Lett. **99**, 190601 (2007).
[65] F. Slanina, Phys. Rev. E **80**, 061135 (2009).
[66] F. Slanina, J. Stat. Phys. **135**, 935 (2009).
[67] D. Chaudhuri and A. Dhar, EPL (Europhys. Lett.) **94**, 30006 (2011).
[68] D. Chaudhuri, A. Raju, and A. Dhar, Phys. Rev. E **91**, 050103 (2015).
[69] J. K. Percus, J. Stat. Phys. **15**, 505 (1976).
[70] U. Seifert, Rep. Prog. Phys. **75**, 126001 (2012).
[71] M. Šiler, T. Čižmár, A. Jonáš, and P. Zemánek, New J. Phys. **10**, 113010 (2008).
[72] R. Di Leonardo, S. Keen, J. Leach, C. D. Saunter, G. D. Love, et al., Phys. Rev. E **76**, 061402 (2007).
[73] A. Curran, A. Yao, G. Gibson, R. Bowman, J. Cooper, et al., J. Biophotonics **3**, 244 (2010).
[74] M. Šiler, T. Čižmár, and P. Zemánek, Appl. Phys. Lett. **100**, 051103 (2012).
[75] V. Ambegaokar and B. I. Halperin, Phys. Rev. Lett. **22**, 1364 (1969).
[76] A. Scala, Phys. Rev. E **86**, 026709 (2012).
[77] P. Maass, M. Dierl, and M. Wolff, in: Diffusive Spreading in Nature, Technology and Society (Eds. A. Bunde, J. Caro, J. Kärger, and G. Vogl) Springer International Publishing, Cham 2018, Chap. 9, p. 147.